THE JOURNAL OF BIOLOGICAL CHEMISTRY
Vol. 272, No. 49, Issue of December 5, pp. 30889–30898, 1997
© 1997 by The American Society for Biochemistry and Molecular Biology, Inc.
Printed in U.S.A.

Low Affinity Interaction of Human or Rat T Cell Adhesion Molecule CD2 with Its Ligand Aligns Adhering Membranes to Achieve High Physiological Affinity*

(Received for publication, August 27, 1997, and in revised form, September 25, 1997)

Michael L. Dustin‡§, David E. Golan¶, De-Min Zhu¶, James M. Miller‡†, Werner Meier‖, Elizabeth A. Davies, and P. Anton van der Merwe****

*From the ‡Center for Immunology and Department of Pathology, Washington University School of Medicine, St. Louis, Missouri 63110, the ¶Departments of Biological Chemistry and Molecular Pharmacology and Medicine, Harvard Medical School, Hematology-Oncology Division, Brigham and Women's Hospital, Boston, Massachusetts 02115, ‖Biogen Incorporated, Cambridge, Massachusetts 02142, and the **Medical Research Council Cellular Immunology Unit, Sir William Dunn School of Pathology, University of Oxford, Oxford OX1 3RE, United Kingdom*

The mechanism by which low affinity adhesion molecules function to produce stable cell-cell adhesion is unknown. In solution, the interaction of human CD2 with its ligand CD58 is of low affinity (500 mM^{-1}) and the interaction of rat CD2 with its ligand CD48 is of still lower affinity (40 mM^{-1}). At the molecular level, however, the two systems are likely to be topologically identical. Fluorescently labeled glycosylphosphatidylinositol-anchored CD48 and CD58 were prepared and incorporated into supported phospholipid bilayers, in which the ligands were capable of free lateral diffusion. Quantitative fluorescence imaging was used to study the binding of cell surface human and rat CD2 molecules to the fluorescent ligands in contact areas between Jurkat cells and the bilayers. These studies provide two major conclusions. First, CD2/ligand interactions cooperate to align membranes with nanometer precision leading to a physiologically effective two-dimensional affinity. This process does not require the intact cytoplasmic tail of CD2. Second, the degree of membrane alignment that can be achieved by topologically similar receptors deteriorates with decreasing affinity. This suggests an affinity limit for the ability of this mode of cooperativity to achieve stable cell-cell adhesion at approximately 10 mM^{-1}.

Many biologically important events are initiated and sustained through low affinity binding interactions in cell-cell and cell-matrix contact areas. Several models suggest that active intracellular mechanisms are engaged to assist these low affinity interactions (1–3). This intracellular regulation can occur through the cytoplasmic domains of the adhesion molecules as in integrins and cadherins (4–6). Other models hypothesize that the ectodomains of low affinity adhesion molecules can oligomerize to produce stable arrays that enhance the intrinsic affinity of the ectodomain interaction (7–9). Testing of these models has been limited by the absence of quantitative affinity measurements in contact areas. The fluid mosaic membrane can be viewed as a nearly two-dimensional solution in which diffusion is constrained to the plane of the membrane, with a small third dimension arising from the flexible tethering of the membrane anchored adhesion molecules (10). The contact area between two apposing membranes may have additional depth in the third dimension due to fluctuations in the distance between the two membranes. The thesis of this study is that low affinity adhesion interactions can succeed in forming many bonds between cells by organizing the two apposing membranes so that the depth of the third dimension is small and optimal for the relevant adhesion molecule pair. When the third dimension is minimized by this cooperativity, the adhesion molecule concentration is increased and bond formation is strongly favored.

In this study, we tested this hypothesis using the human and rat CD2 adhesion systems. CD2 is an adhesion molecule expressed primarily on T lymphocytes in human, rat and other mammalian species. In all species, CD2 is a type I transmembrane protein with two immunoglobulin-like domains and a 115–116-amino acid cytoplasmic tail. The most potent ligand in the human system is CD58 (11, 12). In contrast, CD48 is the CD2 ligand in rats and mice (13). The CD2 cytoplasmic domain is highly conserved, suggesting that rat CD2 would recognize the appropriate cytoplasmic factors in human cells (14). The solution affinity of human CD2 for human CD58 is 500 mM^{-1} at 25 °C, while the affinity of rat CD2 for rat CD48 is 40 mM^{-1} at 25 °C (this study). CD58 and CD48 are structurally very similar; both are glycolipid-anchored molecules with two Ig-like domains and six and five sites of *N*-linked glycosylation, respectively. Rat CD2 has been transfected into human Jurkat T lymphoma cells (15), such that rat and human CD2 can be compared in the same cellular background.

We have previously described a method for determining the number of molecular bonds formed between T cells expressing CD2 and glass-supported planar bilayers bearing laterally mobile, fluorescein-labeled CD58 (16). The binding of CD58 by T cell CD2 is visualized as an accumulation of fluorescence in the contact area. CD2/CD58 binding is dynamic in that the CD58 molecules in the contact area turn over completely every 5–10 min (17). In this study, human Jurkat T cells were used in the native state for studies with human CD2, or were transfected with rat CD2. Bond formation was determined over a wide range of CD58 (human) and CD48 (rat) ligand densities. A recently developed method was used to determine the two-

* This work was supported by a pilot project grant from the Howard Hughes Medical Institute and research grants from Boehringer Ingelheim, Inc. (to M. L. D.), the United Kingdom Medical Research Council (to E. A. D. and P. A. v. d. M.), and the National Institutes of Health (to D. E. G.). The costs of publication of this article were defrayed in part by the payment of page charges. This article must therefore be hereby marked "*advertisement*" in accordance with 18 U.S.C. Section 1734 solely to indicate this fact.

§ To whom correspondence should be addressed: Center for Immunology and Dept. of Pathology, Washington University School of Medicine, 660 S. Euclid Ave., St. Louis, MO 63110.

† Deceased.

dimensional dissociation constants (2D K_d[1] values) for the CD2/ligand interactions.[2] We found that the 2D K_d for interaction of human CD2 with CD58 is 43-fold lower than the 2D K_d for interaction of rat CD2 with CD48. Deletion of the cytoplasmic tail of rat CD2 did not substantially alter the 2D K_d or the efficiency of adhesion. The calculated confinement regions for human CD2/CD58 and rat CD2/CD48 were 3.9–5.5 nm and 15 nm, respectively. The confinement region is a measure of membrane alignment: the smaller the confinement region, the more precisely aligned the apposing membranes. These results strongly support the hypothesis that alignment of apposing membranes by the cooperative activity of CD2/ligand bonds is responsible for the efficiency of CD2/ligand-mediated adhesive interactions in contact areas. The decrease in alignment with decreasing affinity suggests a limit for this mode of cooperativity, and may define an affinity threshold beyond which specific oligomerization or cytoskeletal regulation strategies are required to enhance binding.

EXPERIMENTAL PROCEDURES

Cell Lines and Monoclonal Antibodies—Jurkat cells selected for the ability to produce interleukin-2 in response to T cell receptor (TCR) cross-linking were provided by A. Chan (Washington University, St. Louis, MO). Jurkat cells with low human CD2 expression and transfected with different rat CD2 forms have been described previously (15). Monoclonal antibodies (mAbs) were produced from hybridoma culture supernatants or from ascites produced in SCID mice. TS2/18 is specific for human CD2 (adhesion blocking) (18), TS2/9 for human CD58 (adhesion blocking) (18), OX34 for rat CD2 (adhesion blocking) (19), and OX45 for rat CD48 (adhesion blocking) (20). Fab fragments of TS2/18 were generated by digestion with immobilized papain (21).

Flow Cytometry—Cells were incubated with 50 μg/ml mAbs and then with FITC-conjugated goat anti-mouse IgG (FITC:IgG, 4:1). Cells were washed three times after each staining incubation with antibodies and analyzed on a FACScan (Becton Dickinson, Mountain View, CA). In some experiments adherent cells from planar bilayers were gently eluted by incubation with anti-CD2 mAb, washed, stained as above, and subjected to flow cytometry.

Surface Plasmon Resonance (SPR) Measurements of Rat CD2/CD48 Off-rates and K_d Values—Recombinant rat CD2 was coupled to the BIAcore (Pharmacia, Uppsala, Sweden) flow cell through random primary amines as described previously (22). Unlabeled or FITC-labeled CD48 was injected at a flow rate of 20 μl/min for 6 s, and the SPR response was measured at 25 °C in flow cells with CD2 or a control coating. The specific increase in response units was determined by subtracting the response unit signal on the control surface. Binding data were analyzed as described previously to determine off-rates and K_d values (22).

Labeling of CD48 and CD58—Rat CD48 was purified from rat thymuses on OX45-Sepharose (20). The CD48 was labeled with 8 mM FITC while bound to OX45-Sepharose and eluted at pH 3. Human CD58 was isolated from human erythrocytes on TS2/9-Sepharose (23). The CD58 was labeled with 8 mM FITC while bound to TS2/9-Sepharose and eluted at pH 3. Residual free dye was removed from the protein samples after elution from the affinity columns by ultrafiltration over a M_r 30,000 cut-off membrane (Centricon, Amicon, Danvers, CT). The labeled protein was analyzed by SDS-polyacrylamide gel electrophoresis, followed by fluorescence imaging on a Storm Imager (Molecular Dynamics, San Cupertino, CA). This allowed assessment of both protein purity and absence of free dye, which co-migrated with bromphenol blue. The solution K_d, as analyzed by SPR, of FITC-labeled CD48 binding to rat CD2 (70 μM) was not significantly different from the solution K_d for binding of unlabeled CD48 to CD2 (56 μM) (data not shown). These data are within the range of K_d values determined previously for unlabeled CD48 binding to CD2 that had been immobilized on a sensor chip with a random orientation (22). Thus, the adhesion molecule labeling procedure established originally for human CD58 was shown here to result in full retention of binding activity for rat CD48.

Reconstitution of Fluorescently Labeled CD48 and CD58—Proteins were reconstituted with 0.4 mM egg phosphatidylcholine by detergent dialysis (24). Liposome suspensions were also prepared without added protein (0.4 mM egg phosphatidylcholine only) or with 2 mol% 7-nitro-2–1,3-benzoxadiazol-4-yl (NBD) phosphatidylethanolamine. The initial bilayer preparation contained 2200 molecules/μm^2 CD48 or 1600 molecules/μm^2 CD58 assayed by immunoradiometric methods using iodinated OX45 IgG or TS2/9 IgG, respectively. Dilution of the initial liposome preparation with egg phosphatidylcholine liposomes resulted in a range of FITC-CD48 or FITC-CD58 surface densities that was linear with the dilution factor (data not shown). The fluorescence signal from these bilayers under a standard set of conditions was also linear with surface density, allowing determination of a specific activity in fluorescence (FL) units/molecule (see Table I).

Imaging of CD48 and CD58 Redistribution—Planar bilayers were prepared in a parallel plate flow cell (Bioptechs, Butler, PA). Up to five bilayers could be prepared in one flow cell by sandwiching 1-μl aliquots of liposome suspension between the micro-aqueduct slide and a clean no. 1 coverslip (40 mm diameter). The coverslip and micro-aqueduct slide were separated by a 250-μm silicon rubber gasket such that each bilayer was about 2 mm across. The flow cell was flushed with 5% nonfat dry milk in phosphate-buffered saline and incubated with this solution for at least 20 min at 24 °C. The medium for adhesion assays was Hepes-buffered saline (20 mM Hepes, pH 7.4, 137 mM NaCl, 5 mM KCl, 0.7 mM $NaHPO_4$, 5 mM D-glucose, 2 mM $MgCl_2$, 1 mM $CaCl_2$, 1% bovine serum albumin). In some experiments 1% bovine serum albumin was replaced by 10% fetal bovine serum. Adhesion assays were performed at 24 °C, at which temperature the CD2 adhesion mechanism functioned efficiently. Images of bilayers, cell, and contact areas were acquired using an inverted microscope (Yona Microscopes, Silver Spring, MD). Stable epi-fluorescence illumination was provided by a xenon arc lamp (Opti-Quip, Highland Mills, NY). Images were acquired with a cooled CCD camera (PXL, KAF1400 chip, Photometrics, Tuscon, AZ). The system was interfaced with a computer (Apple, Cupertino, CA) running IP lab software (Signal Analytics, Vienna, VA). Contact areas were directly visualized by interference-reflection microscopy (25). All images were flat-field corrected using averaged images of NBD-phosphatidylethanolamine (2%) bilayers. Images of cells on unlabeled bilayers were always acquired in parallel to allow correction for cell and media autofluorescence.

Normalization of Binding Data to a Single Percent Binding Level—The two-dimensional affinity analysis required that the average number of CD2 molecules per cell (N_t, see Table I for other symbols) was constant over all data points, although at low ligand density the cells with higher cell surface expression of CD2 were selectively bound (see "Results"). The normalization assumed that, when the percentage of cells adhering to a substrate was less than 100%, that the cells with the highest expression of CD2 adhere first. This assumption is consistent with the law of mass action and with data provided under "Results." Normalization therefore required direct determination of the percentage of cells bound at each bilayer density (Π_C). Values of N_b, $B \times p$, and B/F for each contact area at a given initial ligand density were arranged in columns and sorted for decreasing N_b. The highest $(\Pi_{C(low)} \div \Pi_C) \times n$ values were averaged and used to generate a Zhu-Golan plot (see "Results").

Estimation of the Surface Area of Jurkat Cells—The average surface area of the Jurkat cells used in this study was 800 μm^2, based either on the diameter of osmotically swelled cells (average diameter, 16 ± 3.3 μm, n = 86) or on the diameter of cells in isotonic medium (average diameter, 11.4 ± 1.8 μm, n = 25) multiplied by 1.8, a correction factor for the surface roughness of activated T cells (26). For osmotic swelling, the Jurkat cells were resuspended in Hepes-buffered saline diluted 1:9 with water. After 15 min all cells appeared "swelled" and were imaged by differential interference contrast microscopy (DIC); cell diameters were measured using IP Lab software.

Fluorescence Photobleaching Recovery (FPR)—FPR experiments were performed as described previously (17). A focused Gaussian beam from a 2W argon laser (Coherent, Palo Alto, CA) was merged with the xenon arc lamp illumination using a 50% beam splitter. Imaging and bleaching were controlled by an IP Lab script.

Iodination of Soluble CD58 and Direct CD58/CD2 Binding Assays—Soluble human CD58 (sCD58) was purified from supernatants of Chinese hamster ovary (CHO) cells transfected with a construct encoding

[1] The abbreviations used are: 2D K_d, two-dimensional dissociation constant; 3D K_d, three-dimensional dissociation constant; CD, cluster of differentiation; DIC, differential interference contrast; FITC, fluorescein isothiocyanate; FL, fluorescence units; FPR, fluorescence photobleaching recovery; IRM, interference reflection microscopy; LFA, lymphocyte function-associated antigen; NBD, 7-nitro-2–1,3-benzoxadiazol-4-yl; SPR, surface plasmon resonance; TCR, T cell receptor; WT, wild type.

[2] D.-M. Zhu, M. L. Dustin, and D. E. Golan, manuscript in preparation.

TABLE I
Definitions of terms and methods of measurement

Symbol	Definition	Measurement
N_t	Total number of CD2 molecules per cell, averaged over a population of cells	Iodinated IgG or Fab binding
N_b	Total number of bound ligand molecules (molecules/contact)	$B \times S_b$ (see below)
B	Bound ligand density (molecules/μm^2)	$(FL_{contact} - FL_{bilayer} - FL_{autofluor}) \div$ specific activity (FL/molecule)
F	Free ligand density (molecules/μm^2)	$FL_{bilayer} \div$ specific activity (FL/molecule)
S_c	Surface area of cell (μm^2)	$4\pi r^2$, where r is the radius of osmotically swelled cells
S_b	Size of contact area (μm^2)	Interference reflection microscopy (IRM)
p	$S_b \div S_c$	
n	Total number of cells analyzed per bilayer	
C	Initial ligand density (molecules/μm^2)	Immunoradiometric assay on bilayer of known area
f	Fractional mobility	FPR
Π_C	Percentage of cells bound at initial ligand density C	Comparison between IRM (total contacts) and DIC (total cells) images
σ	Confinement region (nm)	(2D $K_d \div$ 3D K_d) $\times$ 1000

truncated, two-Ig domain sCD58 (27). The sCD58 was iodinated with IODOGEN using 1 mCi of ^{125}I/mg of protein. Binding of iodinated sCD58 to Jurkat cells was performed in a 100-μl volume of Hepes-buffered saline/bovine serum albumin at 24 °C. After incubation for 5 min, 90 μl of the cell suspension was transferred to a microsediment tube (Sarstedt) containing 100 μl of oil (1.5 parts dibutylphthalate and 1 part dioctylphthalate). The tube was centrifuged for 3 min at 8000 rpm in a microcentrifuge. The tip containing the cell pellet was cut off using a heated scalpel, and both the tip and top parts of the tube were counted. Nonbound and nonspecifically bound counts in the tip were determined by performing the binding reaction in the presence of 100 μg/ml of TS2/18. The binding data were analyzed both by the method of Scatchard (28) and by using a nonlinear fitting routine (Regression, Blackwell Scientific Publications, Oxford, United Kingdom), with similar results.

RESULTS

A Novel Analysis Method Applies the Law of Mass Action to Interaction of Cell Surface CD2 with Ligands Expressed in Artificial Bilayers—We set out to test the hypothesis that the CD2/ligand interaction aligns membranes, by using a chemical analysis of the CD2/ligand interaction in a model cell-cell contact area. The interaction of human CD2 with CD58 in T-lymphocyte-to-supported-planar-bilayer contact areas is an equilibrium binding process that follows the law of mass action and can thus be described by an affinity constant (16). Because both CD2 and CD58 are tethered to membranes, their concentrations are measured in two-dimensional (surface) units and their interaction is described by a two-dimensional affinity or the reciprocal 2D K_d. Previously we utilized the Scatchard analysis to fit CD2/CD58 binding data and determine the 2D K_d, assuming that all cell surface CD2 molecules were available in the contact area (*i.e.* that the total number if receptors was a constant). However, it is more likely that the movement of laterally mobile CD2, like that of CD58, follows the law of mass action and, at equilibrium, will be distributed between the contact and noncontact areas of the cell membrane. Consistent with this postulate, human CD2 displays a high degree of lateral mobility on Jurkat cells, with a diffusion coefficient (D) of 0.072 μm^2/s and a fractional mobility (f) of 0.7 (29). A novel analytical approach to determining the 2D K_d was developed, using the assumption that the laterally mobile CD2 was available for binding to CD58. The derivation of this analysis will be described in detail elsewhere.[2] The important conceptual feature of the analysis is that the free, laterally mobile CD2 is assumed to diffuse over the entire cell surface. Under these conditions, the following relationship should be satisfied.

$$(B \div F) = [(N_t \times f) \div (K_d \times S_c)] - [(B \times p) \div K_d] \qquad \text{(Eq. 1)}$$

The terms in Equation 1 are defined in Table I. Graphical analysis of this relationship involved plotting $B \times p$ as the abscissa and $B \div F$ as the ordinate for a well distributed series of data points at different ligand densities in the planar bilayer.

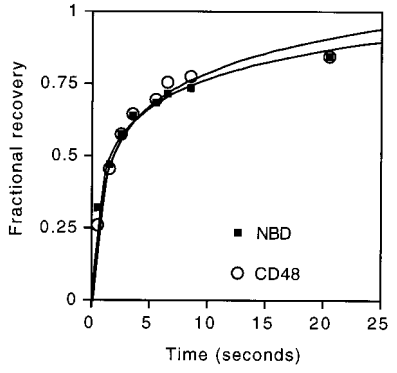

FIG. 1. **Lateral mobility of reconstituted FITC-CD48.** Bilayers containing NBD-phosphatidylethanolamine (*squares*) or FITC-CD48 (*circles*) were prepared in parallel and individually bleached with a 2.8-μm radius laser beam. The time course of fluorescence recovery was followed by using the cooled CCD camera to image the area over a period of 20 s. The *line* represents the best fit of the data to a nonlinear least squares model (17). The lateral mobility of CD48 was not distinguishable from that of the lipid probe. Data are representative of 10 experiments on two bilayer preparations.

The 2D K_d was determined from the negative reciprocal of the slope. The total number of receptor molecules (N_t) on the cell was calculated by the following relationship.

$$N_t = (x \text{ intercept} \times S_c) \div f \qquad \text{(Eq. 2)}$$

For brevity, we will refer to this graphical representation as a "Zhu-Golan plot." This novel analysis required determination of the bound ligand density, the free ligand density, the size of the contact area, and the average surface area of the cell for several different initial ligand densities.

FITC-labeled CD48 Is Laterally Mobile in Supported Planar Bilayers—The novel analysis method assumes that the ligand is freely mobile in the planar bilayer. We have demonstrated previously that FITC-CD58 is laterally mobile in glass-supported planar bilayers (16). The lateral mobility of FITC-CD48 was measured by FPR (17, 30). FITC-CD48 displayed the same fluorescence recovery profile as NBD-phosphatidylethanolamine (2%) in egg phosphatidylcholine bilayers (Fig. 1). The FITC-CD48 had a lateral diffusion coefficient of 1 μm^2/s and a fractional recovery of greater than 90%. This result confirmed that glycosylphosphatidylinositol-anchored CD48 and a model phospholipid interacted identically with bulk lipids in the planar bilayer.

Jurkat T Cells Expressing Rat CD2 Adhere to Planar Bilayers Bearing FITC-CD48—The time course of adhesion mediated by the CD2/CD48 interaction was examined at 24 °C. Bilayers bearing 1500 molecules/μm^2 FITC-CD48 were formed in a parallel plate flow cell. Jurkat T cells expressing rat CD2 were injected into the flow cell and settled on the bilayer. The

time course of CD48 accumulation in the forming contact areas was followed by fluorescence imaging. Accumulation of bound CD48 increased for 15 min at 24 °C and reached a steady state level by 20 min (Fig. 2). This time course was similar to that reported previously for adhesion mediated by human CD2/CD58 on Jurkat cells (16). Both cell adhesion and ligand binding in contact areas were reversed within 10 min by addition of 100 μg/ml OX34 mAb against rat CD2 (data not shown). Jurkat cells lacking rat CD2 did not accumulate FITC-CD48 or adhere to FITC-CD48 bilayers (data not shown).

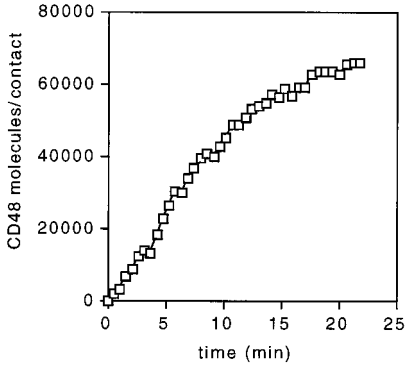

FIG. 2. **Time course of FITC-CD48 accumulation in contact areas between WT rCD2 cells and bilayers.** WT rCD2 cells were injected into a flow cell containing a planar bilayer bearing 1500 molecules/μm^2 FITC-CD48. Images were acquired every 30 s for 22 min at 24 °C. The images were analyzed for specific CD48 binding by subtracting bilayer and cell autofluorescence values and then dividing by the specific activity in FL units/CD48 molecule. Data are representative of three experiments.

Image Analysis of Jurkat Cell Adhesion to FITC-CD58 Bilayers—A key part of the Zhu-Golan analysis is to determine ligand binding over a range of initial ligand densities. The human CD2/CD58 interaction was chosen to illustrate pictorially the multiparameter image collection used to generate these data. Fig. 3 shows representative images of Jurkat T cell adhesion to bilayers containing densities of CD58 ranging from 13 to 200 molecules/μm^2 at 24 °C. The images show pseudocolor representations of fluorescence images calibrated in molecules/μm^2, and images of adherent and nonadherent cells and contact areas in the same field obtained using DIC and interference reflection microscopy (IRM), respectively. Several key features of the interaction are apparent. The percentage of cells forming contacts, the size of the contact area, and the amount of CD58 accumulated all increased with increasing initial density of CD58 in the bilayers. The images of cells on bilayers with no CD58 showed that autofluorescence was low but detectable and relatively uniform, allowing simple subtractive corrections for autofluorescence and bilayer fluorescence to determine the amount of ligand bound in the contact areas (see Table I). The accumulation of FITC-CD58 was rapidly reversed by addition of 100 μg/ml TS2/18 mAb against human CD2. This treatment also reversed contact formation based on IRM imaging. Thus, both the human and rat systems required the CD2/

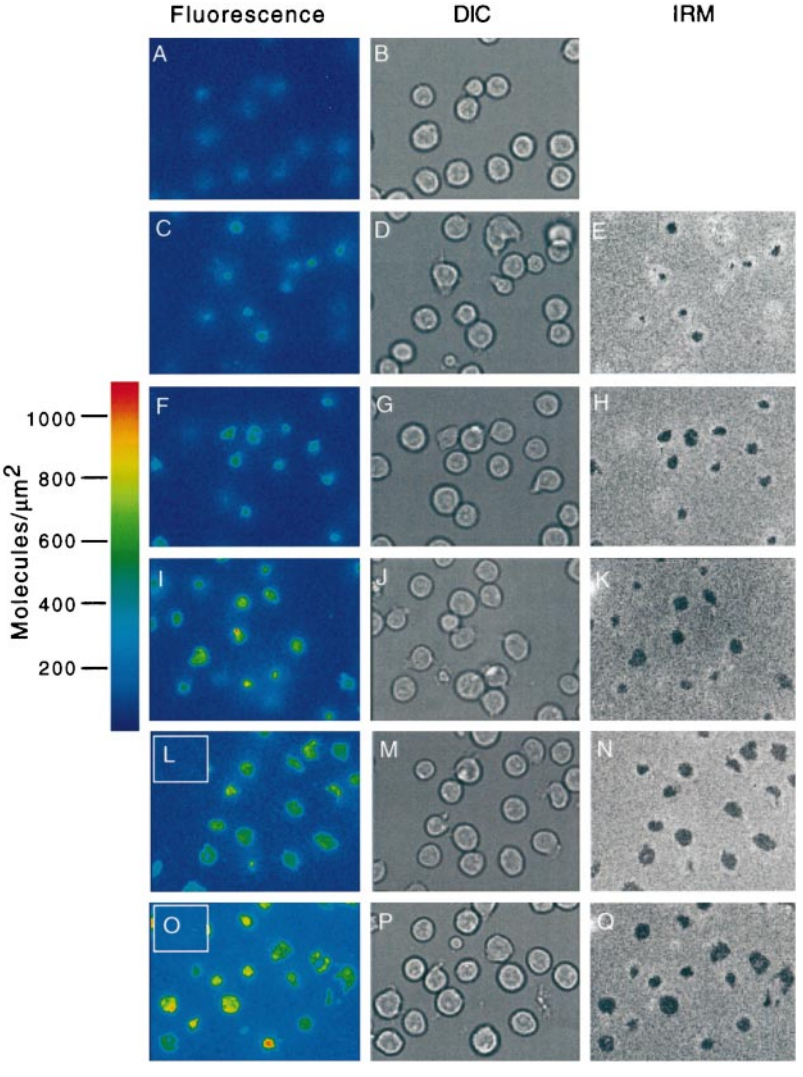

FIG. 3. **Images of Jurkat cells on bilayers bearing different densities of FITC-CD58.** Jurkat cells were injected into a flow cell and allowed to adhere for 30 min at 24 °C. The cells were then imaged over a period of 20 min. The bilayers contained unlabeled CD58 (*A* and *B*), or FITC-CD58 at 13 molecules/μm^2 (*C–E*), 25 molecules/μm^2 (*F–H*), 50 molecules/μm^2 (*I–K*), 100 molecules/μm^2 (*L–N*), or 200 molecules/μm^2 (*O–Q*). Fluorescence images (*A*, *C*, *F*, *I*, *L*, and *O*) were rendered in pseudocolor according to the scale indicated in molecules/μm^2 on the left. The *insets* in the *upper left corners* of *L* and *O* are from images of the bilayers taken prior to injecting cells. Bright field images (*B*, *D*, *G*, *J*, *M*, and *P*) were acquired using DIC optics, but without the DIC analyzer in place to maximize fluorescence signal. Contact area images (*E*, *H*, *K*, *N*, and *Q*) were obtained by IRM. Each image is 91 μm across. Images are representative of three data sets.

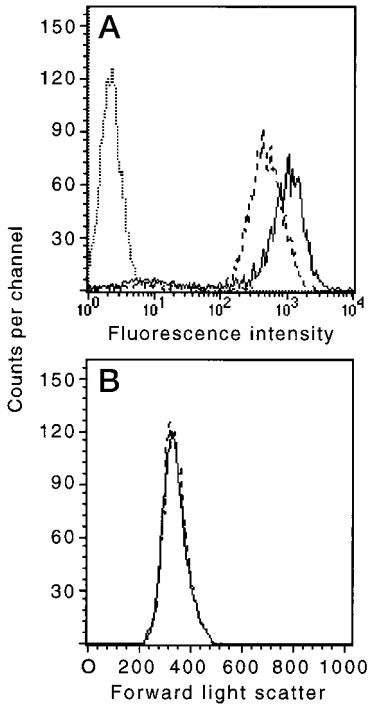

FIG. 4. **Selection of cells expressing higher levels of rat CD2 by bilayers bearing lower densities of CD48.** WT rCD2 cells were incubated on planar bilayers formed on 25 mm diameter round coverslips for 60 min at 24 °C and gently rinsed. Bilayers bearing 1200 or 200 molecules/μm^2 FITC-CD48 were tested. Adherent cells were then incubated with 10 μg/ml OX34 for 30 min, during which time the cells detached spontaneously without application of any shear force. Cells were then incubated with FITC-labeled goat anti-mouse IgG and analyzed on a FACScan (Becton Dickinson, Mountain View, CA). *A*, fluorescence intensity of unstained cells (*dotted line*), cells selected on 1200 molecules/μm^2 CD48 (*dashed line*), or 200 molecules/μm^2 CD48 (*solid line*). Mean fluorescence values: 1200 molecules/μm^2 CD48, 513 FL units; 200 molecules/μm^2 CD48, 1061 FL units. *B*, forward angle light scatter (a parameter related to cell size) of cells selected on 1200 molecules/μm^2 CD48 (*dashed line*) or 200 molecules/μm^2 CD48 (*solid line*). Data are representative of two experiments.

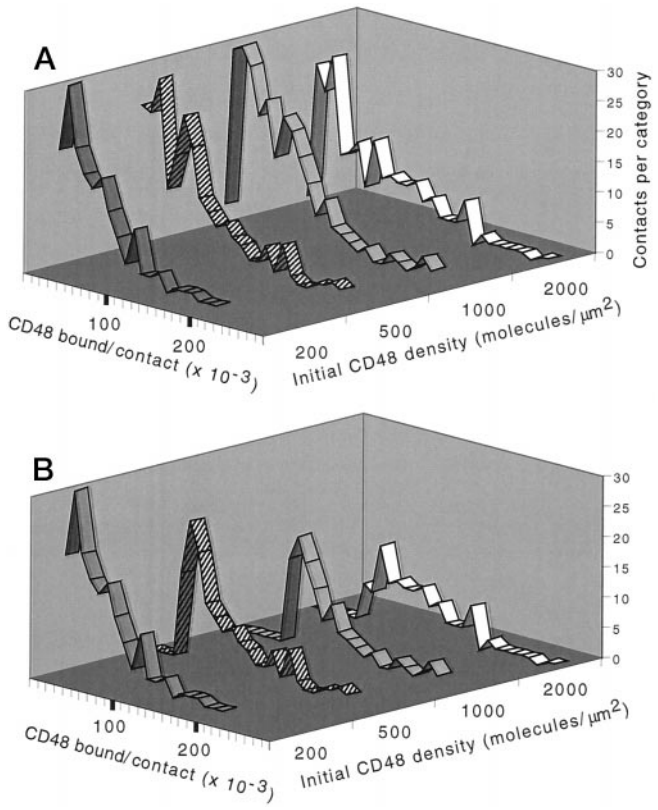

FIG. 5. **Histograms showing the distribution of FITC-CD48 bound by WT rCD2 cells as a function of initial CD48 density.** Contacts were grouped in intervals of 10,000 FITC-CD48 molecules bound per contact area, in which each category includes cells from the indicated value to that value + 9999. *A*, nonselected data, all cells (n) shown. *B*, data selected to 44% adhesion, which was the percentage adhesion actually observed at an initial CD48 density of 220 molecules/μm^2. Note that $(\Pi_{44} \div \Pi_C) \times n$ cells with the highest values of N_b were selected. This normalization resulted in a shift to higher CD48 binding as the degree of selection increased. Data are representative of two experiments for which this analysis was performed.

ligand interaction to achieve contact formation and ligand accumulation.

Bilayers with a Low Density of CD48 Select for Jurkat Cells with a High Density of CD2—To obtain a Zhu-Golan plot with well distributed points, it was necessary to utilize low ligand densities at which a small percentage of cells were adherent. A flow cytometry experiment was performed to determine whether the WT rCD2 cells that adhered selectively at low CD48 density expressed higher levels of CD2. WT rCD2 cells adherent to bilayers bearing 200 molecules/μm^2 rat CD48 expressed, on average, a 2-fold higher level of CD2 than that expressed on cells adherent to bilayers bearing 1200 molecules/μm^2 CD48 (Fig. 4*A*). These data demonstrated that the average amount of CD2 on a population of adherent cells increased as the percent of total cells that were adherent decreased. Because there was no ligand-based selection for cell size (Fig. 4*B*), the increased CD2 expression on cells adherent to low density CD48 bilayers reflected a concomitant increase in CD2 surface density.

Normalization Corrects for Differences in the Average Number of CD2 Molecules per Adherent Cell at Different Ligand Densities—The analysis assumes that the average number of CD2 molecules per adherent cell is equal at all initial ligand densities. Therefore, the result above required that the data sets be normalized to a single level of N_t, based on the assumption that the cells with highest CD2 were preferentially adherent at low initial ligand densities. The effect of this normalization is demonstrated in Fig. 5. Fig. 5*A* shows frequency histograms of total CD48 bound per contact between WT rCD2 cells and four bilayers containing different initial densities of rat CD48. Fig. 5*B* shows the effect of normalization to 44% cell adhesion. The histograms for cells at higher initial CD48 densities were shifted by normalization to higher binding values, *i.e.* all points were brought to the same value of N_t.

Rat CD2 Interaction with CD48 Has a Physiologically Useful 2D K_d—Fig. 6 (*squares*) shows the percent cell adhesion (*A*), average contact size (*B*), and average number of CD48 molecules bound per contact (*C*) for WT rCD2 cell binding to four different initial densities of CD48. The Zhu-Golan plot was used to analyze data normalized to 44% adhesion (Fig. 6*D*). The 2D K_d was calculated to be 47 molecules/μm^2. This affinity is physiologically useful compared with the densities of CD2 and CD48 on rat cells (each >200 molecules/μm^2). The value of N_t derived from this analysis was 140,000 $\div$ f. Because of the normalization procedure, this was the number of cell surface CD2 molecules required for cell adhesion to bilayers bearing 220 molecules/μm^2 FITC-CD48. One important point that could be gleaned from examining the individual contact area data was that as few as 4000 rat CD2/CD48 bonds could maintain a stable contact area (data not shown).

The Cytoplasmic Tail of CD2 Does Not Contribute to the Two-dimensional Affinity—The cytoplasmic domain of CD2 is highly conserved and appears to have a role in regulating adhesion and signaling. Therefore, the effect of truncation of

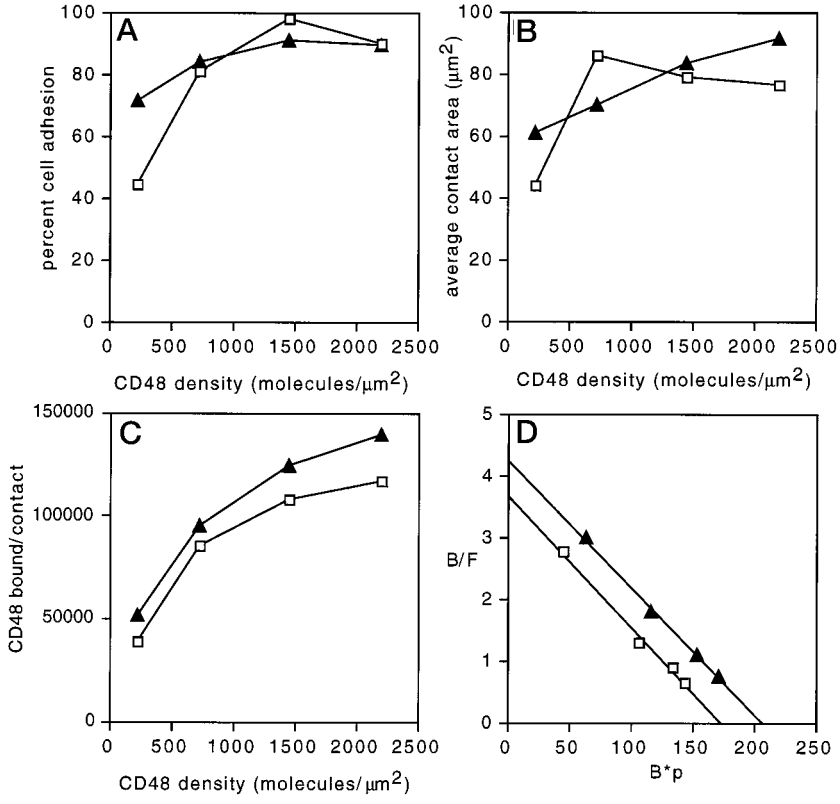

FIG. 6. **FITC-CD48 binding parameters for Jurkat cells expressing WT or cytoplasmic tail truncated rat CD2.** WT rCD2 cells (*squares*) or CY6 rCD2 cells (*triangles*) were injected into a flow cell containing FITC-CD48 bilayers and incubated for 30 min at 24 °C. Images were then acquired on all bilayers over a 20-min period. *A*, percentage of cells bound, based on comparison of DIC and IRM images. *B*, average contact area size, after correction to 44% adhesion. *C*, average number of CD48 molecules bound per contact area, after correction to 44% adhesion. *D*, plot to determine 2D K_d. At least 100 cells were analyzed for each point after normalization to 44% adhesion. Data are representative of three experiments with each type of Jurkat cell.

the CD2 cytoplasmic domain on the 2D K_d for the rat CD2/CD48 interaction was determined. Fig. 6*A* (*triangles*) shows that Jurkat cells expressing 200,000 truncated rat CD2 molecules per cell (CY6 rCD2 cells) bound more efficiently to CD48 bilayers than did WT rCD2 cells. To allow comparison between binding data for WT rCD2 and CY6 rCD2 cells, the CY6 rCD2 data set was also normalized to 44% binding (although 77% of these cells actually adhered at 220 molecules/μm^2 CD48). The contact areas were of similar size (Fig. 6*B*), and the average value of N_b for each bilayer was roughly proportional to the relative amounts of rCD2 ectodomain on the two cell lines (Fig. 6*C*). Fig. 6*D* shows that truncation of most of the cytoplasmic tail of CD2 had no effect on the 2D K_d, which was 47 molecules/μm^2 for the CY6 rCD2 as well as the WT rCD2 cells. The value of Nt was 160,000 ÷ *f* for the CY6 rCD2 cells, similar to that for the WT rCD2 cells. It is important to note that when the data set was normalized to 77% instead of 44% adhesion, the 2D K_d was unchanged at 47 molecules/μm^2 and N_t decreased to 131,000 ÷ *f* (data not shown). Thus, similar numbers of tail-less and wild-type rat CD2 molecules were required for cells to attach to bilayers bearing 220 molecules/μm^2 CD48. We concluded that the cytoplasmic tail of CD2 had little role in determining either the value of the 2D K_d or the total amount of CD2 that was available to bind CD48.

Interaction of Human CD2 with CD58 Has a 43-fold Higher Affinity than Interaction of Rat CD2 with CD48—As described above, the solution affinity of the human CD2/CD58 interaction is higher than that of the rat CD2/CD48 interaction. Jurkat T cells expressing human CD2 were incubated with bilayers containing five different initial densities of FITC-labeled CD58 at 24 °C. Data were analyzed by methods identical to those used for the rat CD2/CD48 interaction. Cell adhesion was half-maximal between 12.5 and 25 molecules/μm^2 FITC-CD58 (Fig. 7*A*), which represented a ligand density 10-fold lower than that required by the rat system for adhesion. The average contact area sizes were generally smaller than those formed by cells using the rat system (compare Figs. 7*B* and 6*B*). The average number of ligand molecules bound per contact was also much lower for the human than for the rat system (compare Figs. 7*C* and 6*C*). The data set was normalized to 30% adhesion for calculation of the 2D K_d. The 2D K_d was 1.1 molecules/μm^2 at 24 °C (Fig. 7*D*), which was 43-fold lower than the 2D K_d for the rat CD2/CD48 interaction in the same cells. The value of N_t was 33,000 ÷ *f*. Another major distinction between the two systems was that stable contacts were formed using as few as 400 bonds in the human system, whereas 4000 rat CD2/CD48 bonds were required to maintain a contact area.

The Normalization Procedure Does Not Affect the 2D K_d—The normalization procedure was designed to extend the analysis to data sets where the percent of adhering cells varied significantly as a function of the initial ligand density, leading to demonstrated variation in N_t for different data points. It was important to demonstrate that the normalization process did not bias the 2D K_d value. Because there was little variation in percent cell adhesion for the three highest initial FITC-CD58 densities, these data points could be plotted without normalization. Fig. 7*D* (*circles*) shows that, in the absence of normalization, there was little change in the slope of the line (K_d = 1.2 molecules/μm^2 without normalization), but a significant change in the value of N_t (21,000 ÷ *f* without normalization). Similar analysis of several experiments using both the human and rat systems demonstrated that the average 2D K_d was not altered by the normalization procedure, but that the confidence limits of the 2D K_d were substantially improved by the additional points that could be included by implementing normalization.

The Solution Affinity for sCD58 Binding to CD2 on Jurkat Cells Agrees with SPR Measurements—The most reliable measurement of CD2 affinity for CD58 has been performed by SPR, where CD58 is covalently coupled to the sensor chip in an oriented manner through its carboxyl-terminal Ig domain. It is also possible to measure K_d values for ligand binding to cells in the low μM range by using centrifugation through an oil cushion to terminate the binding reaction. A set of experiments was

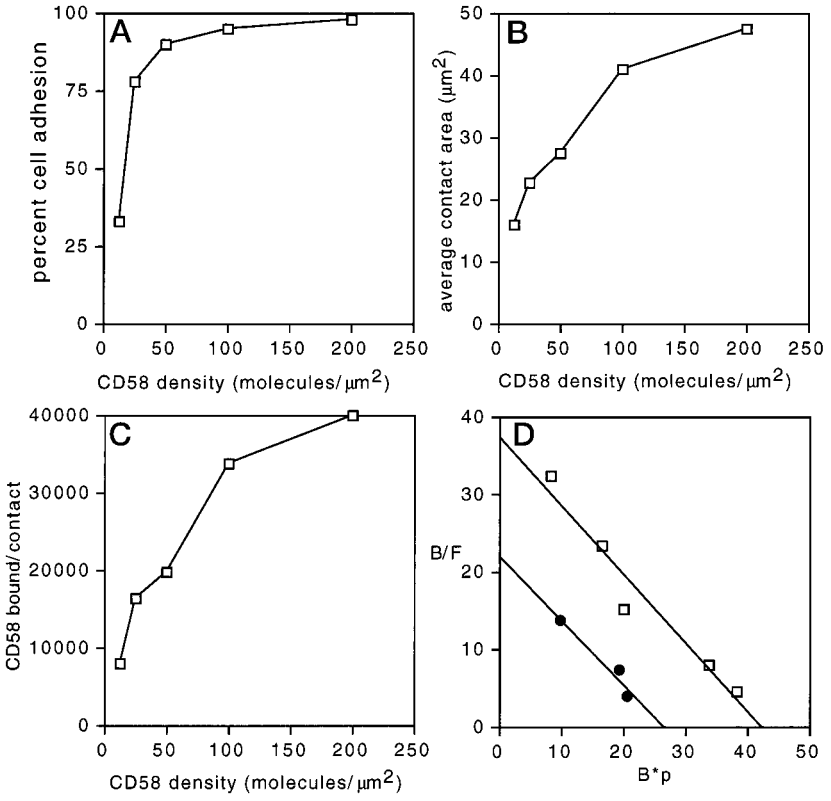

FIG. 7. **FITC-CD58 binding parameters for Jurkat cells expressing human CD2.** Jurkat cells were injected into flow cells containing FITC-CD58 bilayers and incubated for 30 min at 24 °C (*squares*). Images were then acquired on all bilayers over a 20-min period. *A*, percentage of cells bound, based on comparison of DIC and IRM images. *B*, average contact area size after correction to 30% adhesion. *C*, average number of CD58 molecules bound per contact area, after correction as in *B*. *D*, plot to determine 2D K_d. At least 100 cells were analyzed for each point before normalization (*circles*) or after normalization to 30% adhesion (*squares*). Data are representative of two experiments.

performed to examine the solution (3D) K_d for the interaction between monomeric sCD58 and CD2 on Jurkat cells at 24 °C. The binding time was minimized to avoid potential multivalent binding by trace amounts of aggregated sCD58 that could form rapidly following gel filtration and protein concentration. Binding of iodinated sCD58 to Jurkat cells was not detected when the cells were centrifuged through a serum cushion rather than an oil cushion, suggesting that the off-rate was rapid (*i.e.* complete dissociation occurred within 30 s) and that the interaction between CD58 and CD2 was monovalent. A representative data set is shown in Fig. 8. The average K_d was 1.5 μM and the B_{max} was 88,000 receptor sites/cell (n = 10). This 3D K_d was very similar to that measured by SPR (Table II).

The CD2/Ligand Interaction Is Confined to a Nanoscale Space between Cell and Bilayer—Comparison between the solution (3D) K_d and the 2D K_d for the same molecular interaction allows calculation of the confinement region in which the binding sites of the receptor and ligand interact (31).

$$3D\ K_d = 2D\ K_d/\sigma \qquad \text{(Eq. 3)}$$

σ is the confinement region. This analysis is valid if the negative entropic free energy (ΔG_s) of tethering CD2 and CD58 to membranes is not significant compared with the total free energy for the interaction of CD2 and CD58. The loss of one degree of translational (½RT) and two degrees of rotational (RT) free energy due to membrane association is equivalent to 0.89 kcal/mol at 25 °C. In contrast, SPR measurements at 25 °C indicate that the total free energy for interaction of CD2 and ligand in solution is −7.7 kcal/mol and −6.3 kcal/mol for the human and rat systems, respectively. Therefore, the effect of reduced entropic free energy is significant. The appropriate correction for pre-constraining the receptor and ligand to membrane surfaces is to estimate the free energy of interaction of oriented molecules in solution and derive a theoretical 3D K_d from this free energy that is more appropriate for use in Equation 3. The calculated confinement regions were in the range of 3.9–5.5 nm for the human CD2/CD58 and 15 nm for the rat

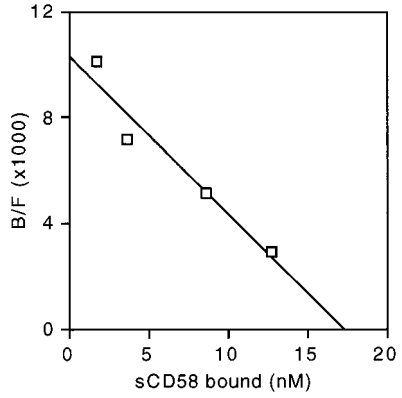

FIG. 8. **Binding of sCD58 to Jurkat cells.** Jurkat cells (~10^7) were incubated with 166 nM, 500 nM, 1.66 μM or 4.34 μM iodinated sCD58 for 5 min at 24 °C, and an aliquot of cells was then centrifuged through a oil cushion. Binding reached equilibrium rapidly at high sCD58 concentrations. Minimizing the binding time reduced the potential for multivalent interactions. Data are representative of eight experiments. The average K_d was 1.5 ± 0.2 μM, and the B_{max} was 88,000 molecules/cell.

CD2/CD48 interaction (Table II). Despite the homology between the human CD2/CD58 and the rat CD2/CD48 systems, then, the confinement region was 4-fold smaller for the human than the rat system. For relatively small, inflexible molecules like CD2 and CD58, σ provides a measure of membrane alignment. Thus, these results suggest that the human CD2/CD58 interaction aligns interacting membranes with ~5-nm precision.

DISCUSSION

In this study we have employed a novel fluorescence microscopy approach to quantify adhesion molecule interactions in model contact areas between T cells and supported phospholipid bilayers. Previously, we applied this approach for the first time to the human CD2/CD58 interaction using a standard Scatchard analysis to estimate the 2D K_d. Here, for the first

TABLE II
Calculation of confinement regions (σ) from solution (3D) and 2D K_d values

For the rat interaction a CD48-CD4 chimera was immobilized via an anti-CD4 antibody (22). For the human interaction CD58 was immobilized via an exposed cysteine in the membrane-proximal domain (11). The gain in affinity due to the negative entropic free energy of linking the ligand to the membrane (ΔG^s) was estimated to be $1.5RT$. This value was added to the calculated free energy (ΔG^s) to determine the predicted 3D K_d for the interaction of oriented molecules in solution (3D K_d*). This value, in turn, was converted to molecules/μm^3 in order to calculate σ.

Molecule	3D K_d	ΔG	$\Delta G + \Delta G^s$	3D K_d*	3D K_d*	2D K_d	σ
	μM	*kcal/mol*	*kcal/mol*	μM	*per* μm^3	*per* μm^2	*nm*
CD58	1.5[a]	−7.9	−8.8	0.34	200	1.1	5.5
CD58	2[b]	−7.7	−8.6	0.47	280	1.1	3.9
CD48	25[b]	−6.3	−7.2	5.1	3100	47	15

[a] One estimate of the 3D K_d for the human CD2/CD58 interaction was obtained by centrifugation of ^{125}I-sCD58-labeled cells through an oil cushion.

[b] 3D K_d values were also obtained by SPR for the rat CD2/CD48 (25 ± 3 μM, $n = 4$) and human CD2/CD58 (2 ± 0.5 μM, $n = 3$) interactions, using CD48 and CD58 immobilized to expose the CD2 binding sites.

time, we employ a refined analytical model and compare the human and rat homologues of the same functional adhesion pathway in terms of a number of parameters including the 2D K_d, which is the physiological K_d for an adhesion mechanism. The human and rat CD2/ligand adhesion mechanisms are topologically similar, yet differ by 12-fold in solution (three-dimensional) affinity, allowing a direct assessment of the role of receptor affinity in adhesion. It has been shown in other systems that adhesion strength is related to adhesion molecule affinity (32, 33). Here we obtain similar results, in that the adhesion pathway with a 12-fold higher K_d requires 10-fold more ligand to reach the same level of adhesion and 10-fold more bonds to maintain a stable contact area. However, the most important new finding is the direct demonstration that adhesion mechanisms of low solution affinity can cooperate to produce contact areas in which alignment of the apposing membranes concentrates the adhesion molecules and generates a high two-dimensional affinity.

We utilize a refined method for calculation of the 2D K_d. The Scatchard analysis we employed previously assumed that the total number of CD2 molecules is in the contact area is a constant (28). However, direct measurements of CD2 lateral mobility (29), and parallel studies on the redistribution of CD2 as a function of CD58 density in bilayers (17)[2] suggest that CD2 is recruited into the contact area by mass action and therefore that the number of CD2 molecules increases over time. The Zhu-Golan analysis introduces the contact area and the surface area of the cell as variables through the dimensionless parameter p.[2] When the data from our earlier paper (16) are re-analyzed using the Zhu-Golan method, the 2D K_d for the human CD2/CD58 interaction is 2 molecules/μm^2, which is similar to the value of the 2D K_d reported here (1.1 molecules/μm^2).

The cooperation of CD2 molecules in generating high physiological affinity appears to be through membrane alignment and not through formation of stable arrays or lateral assemblies. At equilibrium, the highest density of bound ligand achieved in the bilayers is ~1000 molecules/μm^2 for CD58 and 2000 molecules/μm^2 for CD48. These values are neither exceptionally high nor do they constitute organized array formation. Furthermore, photobleaching recovery experiments have demonstrated that the CD58 bound in the contact area is highly dynamic (17), also arguing against a stable array that could be expected to suppress dissociation. We have previously discussed the concept that the degree of tilting of the membrane-tethered protein from the vertical would also increase σ (16). It is likely, however, that heavily glycosylated proteins such as CD2, CD48, and CD58 are supported in an upright position by the steric action of *N*-linked oligosaccharides on the membrane proximal domains, as has been suggested recently for ICAM-2 (34). Along these lines, the most highly conserved *N*-linked glycan of CD2 is positioned at the base of the membrane proximal Ig-like domain (35). Therefore, the most significant variable that is likely to affect σ in this system is the alignment of the apposing membranes. Viewed in this light, σ is a remarkable parameter in that it is derived from two chemical affinity measurements, but reflects a cellular parameter, alignment of apposing membranes, that previously would have been approached by less dynamic measurements such as electron microscopy.

Our major conclusion is based on comparisons of the three-dimensional affinity for an interaction in which the receptor is membrane-bound and the ligand is free in solution, and the two-dimensional affinity for an interaction in which both molecules are tethered to apposing membranes. Here, we relied on SPR data from coupling orientations that are most likely not to interfere with ligand binding. We also measure directly the binding of sCD58 to cells on which CD2 is expressed in its physiological orientation. The latter approach yields a 3D K_d of 1.5 μM, which is very similar to the 3D K_d measured by SPR when CD58 is attached to the sensor chip in an oriented fashion through a free cysteine in the membrane proximal Ig-like domain (11). Quantitative comparison of the 2D K_d and the 3D K_d require a correction for decreased entropy due to membrane anchorage of the ligand. The entropic free energy of membrane tethering is relatively small ($1.5RT$), although, due to the relatively low affinity of the CD2/CD58 and CD2/CD48 interactions, the correction has a large effect (4.4–4.9-fold increase) on the size of the calculated confinement region.

It is of great interest that the cytoplasmic tail-deleted form of rat CD2 has the same 2D K_d and other properties as the wild type form. This suggests that no specific linkages between the CD2 cytoplasmic tail and the cytoskeleton are required for adhesion. However, it is possible that lateral interactions of the CD2 ectodomain or transmembrane domain with other proteins provide linkages to the cytoskeleton that are not altered by removal of the cytoplasmic domain (36). Furthermore, this observation does not rule out a general role of the membrane skeleton in supplying membrane rigidity and thereby helping to distribute forces equally throughout the contact area and to maintain alignment of the membranes (37). The average lateral separation between CD2/ligand bonds in the contact area is quite large; the average separation is 54 nm at the lowest density of bound CD58 and 27 nm at the highest density of bound CD48. By comparison, the Stokes radius of CD58 is about 4.5 nm (38). Given that the average distance between CD2/ligand complexes can be greater than 10 times the value of σ, it may be necessary to stiffen the T cell membrane to maintain efficient membrane alignment. In this regard, it is important to note that the supported bilayer provides an infinitely stiff membrane for presentation of CD58 or CD48 in the present study.

CD2 is a member of an important class of lymphocyte adhesion molecules that are topologically similar to the TCR (13, 39). The TCR must be able to efficiently bind trace levels of peptide major histocompatibility complexes (~10–100 complexes/antigen-presenting cell, corresponding to an average surface density of 0.1 molecules/μm^2) (40, 41). The present study focuses on the nature of the cooperativity by which CD2 self-assembles to efficiently form a stable contact with ligand bearing surfaces. It is reasonable to expect that the TCR/ligand

interaction will also be made more efficient in a contact formed by CD2/ligand interactions (13, 39, 42, 43). As noted above, there is ample space between CD2/CD58 bonds to accommodate other molecules. Therefore, adhesion receptors including CD2 and CD28 may have a dual role in T cell activation. Both of these receptors have potent signaling capabilities that synergize with TCR signaling in different contexts (44–47). Under conditions of limiting antigen, however, we predict an additional role for these receptors: allowing TCRs to capture rare major histocompatibility complex-peptide complexes and sequester the complexes in a stable contact cap, where the TCRs can maintain signaling over the extended period of time required for full T cell activation (39, 42, 43).

Interactions of membrane-tethered proteins can occur either between molecules on different membranes (trans) or between molecules on the same membrane (cis). The size of σ for cis interactions is likely to be governed more by molecular flexibility and topology than by affinity, since it is not necessary to use the affinity of the molecular interaction to align two apposing membranes. Interactions in the plane of the membrane involved in such processes as signaling and receptor-mediated endocytosis are therefore likely to function with lower intrinsic affinities than membrane-membrane adhesive interactions. For example, regulation of Src family kinases by SH3 domain displacement requires millimolar concentrations of competing peptides in solution (48). If the protein carrying the SH3 binding peptide were membrane-tethered like the Src kinase and co-confined to a nanometer-scale space with the binding surface of the SH3 domain, then the predicted 2D K_d would be $\sim$600 molecules/μm^2, which is a readily attainable density for proteins on the inner surface of the cell membrane.

The interaction of adhesion molecules in contact areas between cells provides the "raw material" for regulated adhesion. Our results demonstrate that the interaction of CD2 and CD58 is very efficient once a precise alignment of the two apposing membranes is established. The alignment of membranes is tighter for the higher affinity human CD2/CD58 interaction than for the rat CD2/CD48 interaction. We speculate that the 40 mM^{-1} solution affinity of the rat CD2/CD48 interaction is functioning near the natural limit for this cooperative process. An interaction of lower affinity than that of rat CD2/CD48 might be unable to establish the necessary alignment of the apposing membranes in the nascent contact to generate a stable, cooperative contact area. We propose further that an interaction of lower affinity than that of CD2/CD48 could render the adhesion mechanism dependent on a higher level of molecular organization, such as that imposed by the cytoskeleton or by the formation of two-dimensional arrays. For example, a glycosylphosphatidylinositol-anchored form of the LFA-1 I domain binds ICAM-1 with an affinity of $\sim$10 mM^{-1} and does not form stable contact areas on ICAM-1 substrates, but does display rolling adhesion confirming that transient molecular interactions take place (49). One important conclusion of this study is that the relationship between the 2D and 3D K_d values is nonlinear, because σ appears to increase with 3D K_d.

Is the CD2/CD58 interaction modulated by intracellular mechanisms? CD2-mediated adhesion may be regulated by adhesion molecule lateral mobility. Ligand lateral mobility has been shown to have a profound effect on CD2-mediated adhesion (50). It has also been shown that the mobile fraction of antibody-ligated CD2 decreases following T cell activation, but the relationship of this partial immobilization to adhesion regulation is not known (29). Regulation of lateral mobility has been proposed to regulate the initial interaction of LFA-1 and ICAM-1 (51). In this example, LFA-1 is laterally immobilized and essentially inactive for binding ligand. Cell activation or treatment with a low concentration of cytochalasin D results in release of LFA-1 from inhibitory cytoskeletal interactions and in increased collisions with ICAM-1, leading to adhesion (51). Bierer and colleagues (44) have reported that T cell activation leads to increased T cell adhesion to laterally immobile CD58. When the CD58 is immobile the lateral diffusion of cellular CD2 could become a critical parameter, and regulation of CD2 lateral diffusion could account for the observed increase in adhesion upon T cell activation. In our studies, the rapid lateral mobility of the ligand in the planar bilayers could overcome any effect of regulating CD2 mobility on initial ligand binding. Nonetheless, receptor immobilization may be a mechanism to suppress the activity of adhesion mechanisms like CD2/CD58 that, when laterally mobile, cooperate to align membranes and form many transient bonds.

Acknowledgments—M. L. D. thanks E. Unanue for continued support and A. Shaw for discussions on Src kinase activation. We thank E. Elson for the use of the argon ion laser and for general discussions on physical aspects of biological membranes. We thank Yona Nissim for his work on our imaging system and suggesting several important improvements that made this study possible. We thank D. Leckband and H. Erickson for discussions on entropic free energy calculations.

REFERENCES

1. Ward, M. D., Dembo, M., and Hammer, D. A. (1994) *Biophys. J.* **67,** 2522–2534
2. Burridge, K., Fath, K., Kelly, T., Nuckolls, G., and Turner, C. (1988) *Annu. Rev. Cell Biol.* **4,** 487–525
3. Takeichi, M. (1990) *Annu. Rev. Biochem.* **59,** 237–252
4. Nagafuchi, A., and Takeichi, M. (1988) *EMBO J.* **7,** 3679–3684
5. Hibbs, M. L., Xu, H., Stacker, S. A., and Springer, T. A. (1991) *Science* **251,** 1611–1613
6. O'Toole, T. E., Katagira, Y., Faull, R. J., Peter, K., Tamura, R., Quaranta, V., Loftus, J. C., Shattil, S. J., and Ginsberg, M. H. (1994) *J. Cell Biol.* **124,** 1047–1059
7. Shapiro, L., Fannon, A. M., Kwong, P. D., Thompson, A., Lehman, M. S., Grübel, G., Legrand, J. F., Als-Nielsen, J., Colman, D. R., and Hendrickson, W. A. (1995) *Nature* **374,** 327–337
8. Shapiro, L., Doyle, J. P., Hensley, P., Coleman, D. R., and Hendrickson, W. A. (1996) *Neuron* **17,** 435–449
9. Sakihama, T., Smolyar, A., and Reinherz, E. L. (1995) *Immunol. Today* **16,** 581–587
10. Singer, S. J., and Nicolson, G. L. (1972) *Science* **175,** 720–731
11. van der Merwe, P. A., Barclay, A. N., Mason, D. W., Davies, E. A., Morgan, B. P., Tone, M., Krishnam, A. K. C., Ianelli, C., and Davis, S. J. (1994) *Biochemistry* **33,** 10149–10160
12. Sandrin, M. S., Mouhtouris, E., Vaughan, H. A., Warren, H. S., and Parish, C. R. (1993) *J. Immunol.* **151,** 4606–4613
13. Davis, S. J., and van der Merwe, P. A. (1996) *Immunol. Today* **17,** 177–187
14. Melton, E., Sarner, N., Torkar, M., van der Merwe, P. A., Russell, J. Q., Budd, R. C., Mamlaki, C., Tolaini, M., Kioussis, D., and Zamoyska, R. (1996) *Eur. J. Immunol.* **26,** 2952–2963
15. He, Q., Beyers, A. D., Barclay, A. N., and Williams, A. F. (1988) *Cell* **54,** 979–984
16. Dustin, M. L., Ferguson, L. M., Chan, P. Y., Springer, T. A., and Golan, D. E. (1996) *J. Cell Biol.* **132,** 465–474
17. Dustin, M. L. (1997) *J. Biol. Chem.* **272,** 15782–15788
18. Sanchez-Madrid, F., Krensky, A. M., Ware, C. F., Robbins, E., Strominger, J. L., Burakoff, S. J., and Springer, T. A. (1982) *Proc. Natl. Acad. Sci. U. S. A.* **79,** 7489–7493
19. Williams, A. F., Barclay, A. N., Clark, S. J., Paterson, D. J., and Willis, A. C. (1987) *J. Exp. Med.* **165,** 368–380
20. van der Merwe, P. A., McPherson, D. C., Brown, M. H., Barclay, A. N., Cyster, J. G., Williams, A. F., and Davis, S. J. (1993) *Eur. J. Immunol.* **23,** 1373–1377
21. Parham, P., Androlewicz, M. J., Brodsky, F. M., Holmes, N. J., and Ways, J. P. (1982) *J. Immunol. Methods* **53,** 133–173
22. van der Merwe, P. A., Brown, M. H., Davis, S. J., and Barclay, A. N. (1993) *EMBO J.* **12,** 4945–4954
23. Dustin, M. L., Sanders, M. E., Shaw, S., and Springer, T. A. (1987) *J. Exp. Med.* **165,** 677–692
24. Mimms, L. T., Zampighi, G., Nozaki, Y., Tanford, C., and Reynolds, J. A. (1981) *Biochemistry* **20,** 833–840
25. Izzard, C. S., and Lochner, L. (1976) *J. Cell Sci.* **21,** 129–159
26. Mege, J. L., Capo, C., Benoliel, A. M., Foa, C., Galindo, R., and Bongrand, P. (1986) *J. Theor. Biol.* **119,** 147–160
27. Miller, G. T., Hochman, P. S., Meier, W., Tizard, R., Bixler, S. A., Rosa, M. D., and Wallner, B. P. (1993) *J. Exp. Med.* **178,** 211–222
28. Scatchard, G. (1949) *Ann. N. Y. Acad. Sci.* **51,** 660–672
29. Liu, S. J., Hahn, W. C., Bierer, B. E., and Golan, D. E. (1995) *Biophys. J.* **68,** 459–470
30. Axelrod, D., Koppel, D. E., Schlessinger, J., Elson, E. L., and Webb, W. W. (1976) *Biophys. J.* **16,** 1055–1069
31. Bell, G. I., Dembo, M., and Bongrand, P. (1984) *Biophys. J.* **45,** 1051–1064
32. Kuo, S. C., and Lauffenburger, D. A. (1993) *Biophys. J.* **65,** 2191–2200
33. Palecek, S. P., Loftus, J. C., Ginsberg, M. H., Lauffenburger, D. A., and

Horwitz, A. F. (1997) *Nature* **385,** 537–540
34. Casasnovas, J. M., Springer, T. A., Liu, J., Harrison, S. C., and Wang, J. (1997) *Nature* **387,** 312–315
35. Tavernor, A. S., Kydd, J. H., Bodian, D. L., Jones, E. Y., Stuart, D. I., Davis, S. J., and Butcher, G. W. (1994) *Eur. J. Biochem.* **219,** 969–976
36. Varhagen, A. M., Schraven, B., Wild, M., Wallich, R., and Meuer, S. C. (1996) *Eur. J. Immunol.* **26,** 2841–2849
37. Trinkaus, J. P. (1984) *Cells into Organs: The Forces That Shape The Embryo*, Prentice-Hall, Inc., Englewood Cliffs, NJ
38. Dustin, M. L., Olive, D., and Springer, T. A. (1989) *J. Exp. Med.* **169,** 503–517
39. van der Merwe, P. A., McNamee, P. N., Davies, E. A., Barclay, A. N., and Davis, S. J. (1995) *Curr. Biol.* **5,** 74–84
40. Harding, C. V., and Unanue, E. R. (1990) *Nature* **346,** 574–576
41. Kageyama, S., Tsomides, T. J., Sykulev, Y., and Eisen, H. N. (1995) *J. Immunol.* **154,** 567–576
42. van der Merwe, P. A., and Barclay, A. N. (1994) *Trends Biochem. Sci.* **19,** 354
43. Shaw, A. S., and Dustin, M. L. (1997) *Immunity* **6,** 361–369
44. Hahn, W. C., Rosenstein, Y., Calvo, V., Burakoff, S. J., and Bierer, B. E. (1992) *Proc. Natl. Acad. Sci. U. S. A.* **89,** 7179–7183
45. Bell, G. M., Fargnoli, J., Bolen, J. B., Kish, L., and Imboden, J. B. (1996) *J. Exp. Med.* **183,** 169–178
46. Ward, S. G., June, C. H., and Olive, D. (1996) *Immunol. Today* **17,** 187–197
47. June, C. H., Ledbetter, J. A., Linsley, P. S., and Thompson, C. B. (1990) *Immunol. Today* **11,** 211–216
48. Moarefi, I., LaFevre-Bernt, M., Sicheri, F., Huse, M., Lee, C. H., Kuriyan, J., and Miller, W. T. (1997) *Nature* **385,** 650–653
49. Knorr, R., and Dustin, M. L. (1997) *J. Exp. Med.* **186,** 719–730
50. Chan, P. Y., Lawrence, M. B., Dustin, M. L., Ferguson, L. M., Golan, D. E., and Springer, T. A. (1991) *J. Cell Biol.* **115,** 245–255
51. Kucik, D. F., Dustin, M. L., Miller, J. M., and Brown, E. J. (1996) *J. Clin. Invest.* **97,** 2139–2144